Published OnlineFirst March 2, 2016; DOI: 10.1158/1078-0432.CCR-15-1698

Cancer Therapy: Preclinical

Clinical Cancer Research

Targeting MDM2 for Treatment of Adenoid Cystic Carcinoma

Kristy A. Warner[1], Felipe Nör[1,2], Gerson A. Acasigua[1,2], Manoela D. Martins[2,3], Zhaocheng Zhang[1], Scott A. McLean[4,5], Matthew E. Spector[4,5], Douglas B. Chepeha[6], Joseph Helman[5,7], Michael J. Wick[8], Christopher A. Moskaluk[9], Rogerio M. Castilho[3], Alexander T. Pearson[1,5,10], Shaomeng Wang[5,10,11,12], and Jacques E. Nör[1,4,5,13]

Abstract

Purpose: There are no effective treatment options for patients with advanced adenoid cystic carcinoma (ACC). Here, we evaluated the effect of a new small molecule inhibitor of the MDM2–p53 interaction (MI-773) in preclinical models of ACC.

Experimental Design: To evaluate the anti-tumor effect of MI-773, we administered it to mice harboring three different patient-derived xenograft (PDX) models of ACC expressing functional p53. The effect of MI-773 on MDM2, p53, phospho-p53, and p21 was examined by Western blots in 5 low passage primary human ACC cell lines and in MI-773-treated PDX tumors.

Results: Single-agent MI-773 caused tumor regression in the 3 PDX models of ACC studied here. For example, we observed a tumor growth inhibition index of 127% in UM-PDX-HACC-5 tumors that was associated with an increase in the fraction of apoptotic cells ($P = 0.015$). The number of p53-positive cells was increased in MI-773-treated PDX tumors ($P < 0.001$), with a correspondent shift in p53 localization from the nucleus to the cytoplasm. Western blots demonstrated that MI-773 potently induced expression of p53 and its downstream targets p21, MDM2, and induced phosphorylation of p53 (serine 392) in low passage primary human ACC cells. Notably, MI-773 induced a dose-dependent increase in the fraction of apoptotic ACC cells and in the fraction of cells in the G_1 phase of cell cycle ($P < 0.05$).

Conclusions: Collectively, these data demonstrate that therapeutic inhibition of the MDM2–p53 interaction with MI-773 activates downstream effectors of apoptosis and causes robust tumor regression in preclinical models of ACC. *Clin Cancer Res; 22(14); 3550–9. ©2016 AACR.*

Introduction

Adenoid cystic carcinoma (ACC) is one of the two most common malignant salivary gland tumors (1). ACC presents with three different histologic growth patterns. Tubular is the least aggressive, followed by cribriform, and most aggressive is the solid growth pattern (1). Perineural invasion and metastatic spread to distant sites (bones, lungs) are frequently seen in these patients and contribute to poor long-term prognosis (1–4). Although the primary site can be controlled in approximately 30% of ACC patients, they tend to develop distant metastasis and succumb to their disease (5). The standard treatment for these patients is surgery followed by radiation (5, 6). Systemic chemotherapy treatment has been attempted (e.g., cisplatin, paclitaxel, doxorubicin); however, these therapies have low responsive rates (5, 6). An effective systemic therapeutic intervention is required to improve outcomes for patients with ACC.

The function of the tumor suppressor p53 can be inactivated by gene deletion or mutation (7); however, many tumors exhibit wild-type and fully active p53. When p53 is not mutated, its ability to regulate cellular growth, initiate apoptosis, and repair DNA is prevented by the direct interaction with murine double minute (MDM)-2 (8). The proto-oncogene MDM2 was first identified in a spontaneously transformed mouse cell line, and functions as a key negative regulator of p53 that "marks" it for polyubiquitination and degradation through the 26S proteasomal pathway (8, 9). Several studies have reported the expression and function of p53 and MDM2 in malignant salivary gland tumors (10–14). Indeed, it has been suggested that MDM2 participates in ACC tumorigenesis (10, 13, 14), providing a scientific rationale for therapeutic targeting of the MDM2–p53 interaction in these tumors.

[1]Department of Cariology, Restorative Sciences, Endodontics, University of Michigan School of Dentistry, Ann Arbor, Michigan. [2]Department of Oral Pathology, Universidade Federal do Rio Grande do Sul, Porto Alegre, RS, Brazil. [3]Department of Periodontics and Oral Medicine, University of Michigan School of Dentistry, Ann Arbor, Michigan. [4]Department of Otolaryngology, University of Michigan School of Medicine, Ann Arbor, Michigan. [5]University of Michigan Comprehensive Cancer Center, Ann Arbor, Michigan. [6]Department of Otolaryngology, University of Toronto, Ontario, Canada. [7]Department of Oral and Maxillofacial Surgery, University of Michigan School of Dentistry, Ann Arbor, Michigan. [8]South Texas Accelerated Research Therapeutics, San Antonio, Texas. [9]Department of Pathology, University of Virginia, Charlottesville, Virginia. [10]Department of Internal Medicine, University of Michigan School of Medicine, Ann Arbor, Michigan. [11]Department of Pharmacology, University of Michigan School of Medicine, Ann Arbor, Michigan. [12]Department of Medicinal Chemistry, University of Michigan College of Pharmacy, Ann Arbor, Michigan. [13]Department of Biomedical Engineering, University of Michigan College of Engineering, Ann Arbor, Michigan.

Note: Supplementary data for this article are available at Clinical Cancer Research Online (http://clincancerres.aacrjournals.org/).

Corresponding Author: Jacques E. Nör, University of Michigan School of Dentistry, 1011 N. University Rm. 2353, Ann Arbor, MI 48109-1078. Phone: 734-936-9300; Fax: 734-936-1597; E-mail: jenor@umich.edu

doi: 10.1158/1078-0432.CCR-15-1698

Published OnlineFirst March 2, 2016; DOI: 10.1158/1078-0432.CCR-15-1698

Translational Relevance

There are no safe and effective therapies for advanced adenoid cystic carcinoma. Adenoid cystic carcinoma is typically treated with surgery and adjuvant radiation. However, even if the primary site is controlled, patients frequently succumb to distant disease. Despite multiple clinical trials, there is no effective chemotherapeutic for the recurrent/metastatic population. Here, we unveil the therapeutic efficacy of a new small molecule inhibitor of the MDM2–p53 interaction (MI-773) in preclinical models of adenoid cystic carcinoma. We show robust tumor regression in three patient-derived xenograft (PDX) tumor models of adenoid cystic carcinoma, and demonstrate that the mechanism of tumor regression is associated with MI-773–induced tumor cell apoptosis. Collectively, these data suggest that patients with adenoid cystic carcinoma might benefit from therapeutic inhibition of MDM2–p53 interaction.

We have recently reported the isolation and propagation of tumorigenic mucoepidermoid carcinoma cell lines (15). Using collagenase-hylauronidase to digest human tumors, we were able to establish these tumorigenic cells *in vitro* using an optimal culture medium and *in vivo* in xenograft tumors. Similar approaches with human ACC tumors have failed to establish authentic, tumorigenic ACC cell lines. The Tetsu laboratory reported contamination and misidentification of six established ACC cell lines (16). They were determined to be HeLa cells (ACC2, ACC3, ACCM), T24 bladder cancer cells (ACCS) or derived from mouse (ACCNS) or rat (CAC2). The Queimado laboratory was able to establish ACC cell lines upon immortalization with HPV16 E6/E7 under a MMLV promoter (17), but these cells were nontumorigenic. Similarly, the El-Naggar laboratory developed an ACC cell line that was immortalized with human telomerase transcriptase (htert) that is nontumorigenic when transplanted *in vivo* (18). We have attempted to generate tumorigenic ACC cell lines without success so far, and therefore the work presented here utilizes low passage primary ACC cells retrieved from surgical specimens for *in vitro* studies. Recently, the Moskaluk laboratory was able to develop and characterize xenograft model systems for the study of ACC *in vivo* (19) upon direct transplantation of human ACC tumor tissues into immunodeficient mice. We used a similar approach to establish a patient derived xenograft model (PDX) of ACC, that is UM-PDX-HACC-5. In addition to our in-house model, we also used the ACCx6 and ACCx9 models established by the Moskaluk laboratory (19) for the developmental therapeutic studies included here.

The Wang laboratory has recently developed a new class of small molecule inhibitors of the MDM2–p53 interaction. They have reported that MDM2 inhibitors induce tumor cell apoptosis and inhibit xenograft (e.g., osteosarcoma, prostate, and colon cancer) tumor growth (20–23). Indeed, MI-773 (SAR405838) has advanced into phase I clinical trials for cancer treatment (20). MI-773 binds to MDM2 with high affinity (K_i = 0.88 nmol/L) and blocks the p53–MDM2 interaction (20). Consequently, MI-773 inhibits MDM2-mediated p53 protein degradation resulting in p53 accumulation, activates downstream transcription of p53-targeted genes (e.g., MDM2, p21), and causes apoptotic cell death. However, it is unclear if MI-773 can overcome the typical resistance to therapy observed in ACCs. The purpose of this study was to evaluate the antitumor effect of single agent MI-773 in preclinical models of ACC.

Materials and Methods

Low passage primary human ACC cells

Patients with ACC were recruited and consented with the University of Michigan Head and Neck SPORE consent form that was reviewed and approved by our institutional review board (IRB). Human ACC tumors were minced and digested to generate primary cell cultures, as previously described (15). In contrast to mucoepidermoid carcinomas that were amenable to the spontaneous establishment of immortalized cell lines, the ACC cells used here could be expanded to <20 passages, and therefore are considered low passage primary ACC cells. These primary ACC cells were named the University of Michigan-Human ACC (UM-HACC) series (Supplementary Table S1), and were grown in a salivary gland culture medium (SGM) consisting of high glucose Dulbecco's Modified Eagle Medium (DMEM; Invitrogen) supplemented with 2 mmol/L L-glutamine (Invitrogen), 1% antibiotic (AAA; Sigma-Aldrich), 10% FBS, 20 ng/mL epidermal growth factor (Sigma-Aldrich), 400 ng/mL hydrocortisone, 5 μg/mL insulin, 50 ng/mL nystatin, and 1% amphotericin B (Sigma-Aldrich). UM-HACC-1 cells were derived from a tumor that presented with perineural invasion. UM-HACC-2A cells were derived from an aggressive primary tumor, which presented with a lymph node metastasis (UM-HACC-2B cells). UM-HACC-5 cells were derived from a patient that had perineural and bone invasion at the time of surgery. Cells derived from the UM-HACC-6 patient grew from a recurrent tumor that presented with perineural invasion approximately 15 years after initial diagnosis and treatment, reflecting the slow but aggressive course of ACC. In confirmatory studies, we used 2 additional PDX models of ACC: ACCx6 derived from a lung metastasis and ACCx9 derived from a primary tumor located in the parotid gland (Supplementary Table S1) that were generated and fully characterized in the Moskaluk laboratory (19).

Patient-derived xenograft ACC models

To establish a patient-derived xenograft (PDX) model of ACC, human tumor fragments from the UM-HACC-5 patient were transplanted subcutaneously into the dorsal region of male severe combined immunodeficient (SCID) mice (CB.17.SCID; Charles River). Two of six initial patient tumor fragments transplanted, grew, and were retransplanted *in vivo* into new male or female mice for up to 12 passages. When tumors reached an average of 250 mm^3, mice were randomized into groups and received either vehicle (polyethylene glycol-200 + D-α-tocopherol polyethylene glycol 1000 succinate; Sigma-Aldrich), or treatment with 10, 50, or 100 mg/kg MI-773 daily by oral gavage. The Institutional Animal Care and Use Committee of the University of Michigan reviewed and approved these procedures. The ACCx6 and ACCx9 models were treated with vehicle or 100 mg/kg MI-773 at South Texas Accelerated Research Therapeutics (START) using the same protocol as described above.

Patient, xenograft tumor, and primary ACC tumor cell authentication

To validate identification of UM-HACC-1,-2A,-2B,-5, and -6 cells, genomic DNA was extracted using the Wizard Genomic DNA Purification Kit (Promega). DNA genotyping by short

Published OnlineFirst March 2, 2016; DOI: 10.1158/1078-0432.CCR-15-1698

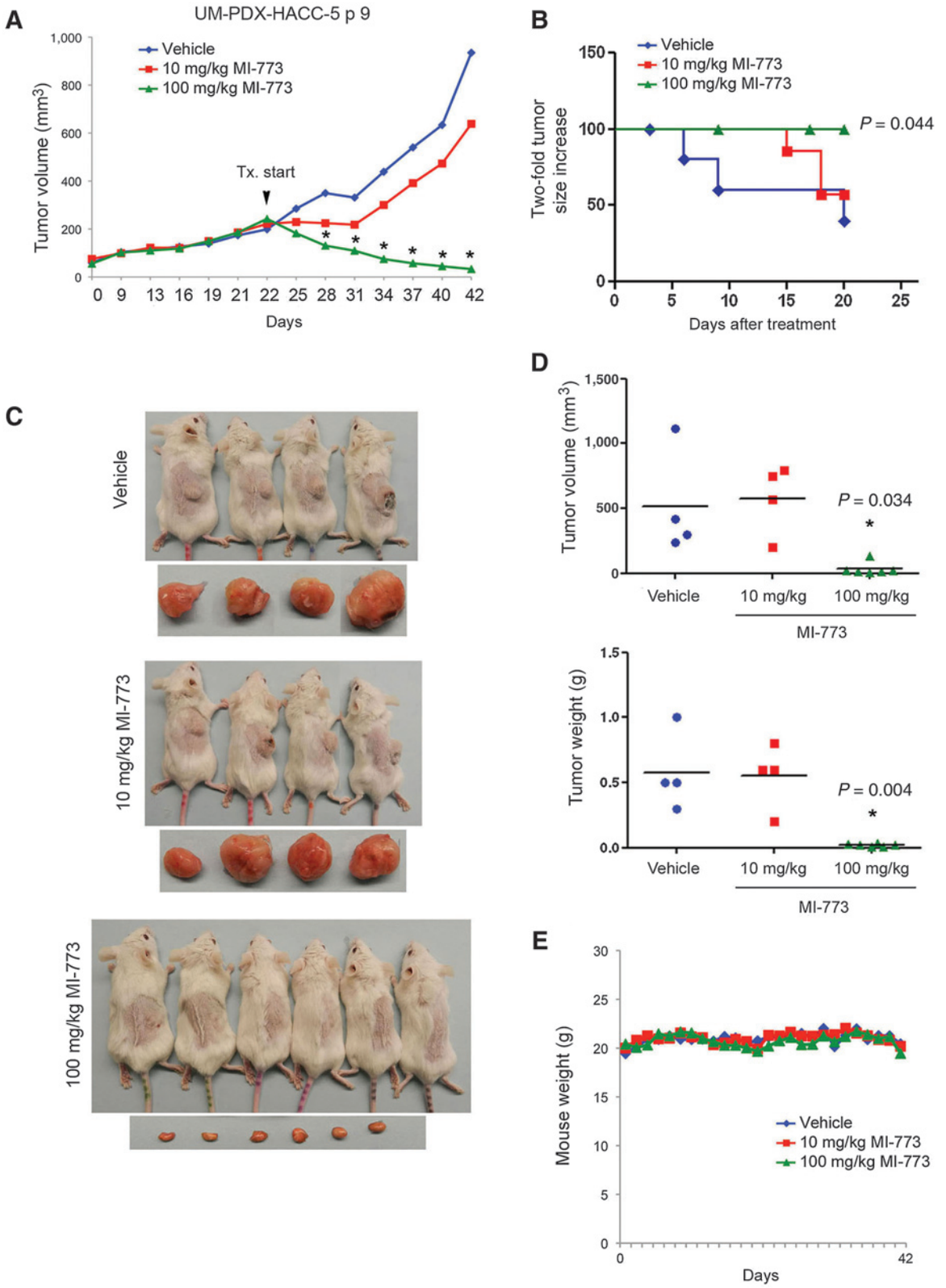

Published OnlineFirst March 2, 2016; DOI: 10.1158/1078-0432.CCR-15-1698

tandem repeat (STR) profiling was performed and analyzed independently by Genetica DNA Laboratories (Burlington, NC) for each matching human tumor, xenograft tumor, and low passage cells. STR profiling confirmed the identity of the low passage primary ACC cells and UM-HACC-5 PDX model (Supplementary Table S2).

Gene sequencing, Western blot, immunohistochemistry, *in situ* TUNEL staining, and FISH

DNA was extracted from the UM-HACC-5 patient saliva and tumor tissue, UM-PDX-HACC-5 tumors (passages 9,12), low passage primary human ACC cells UM-HACC-1 (p11), UM-HACC-5 (p8), UM-HACC-6 (p7), UM-HACC-2A (p6), and analyzed for p53 mutations at the University of Michigan DNA Sequencing Core. Sequences were analyzed using the BLAST tool from the National Center for Biotechnology Information (blast.ncbi.nim.nih.gov). Amino acid sequences were generated using ExPASy online tool (Swiss Institute of Bioinformatics). RNA was extracted with TRizol and protein was extracted with NP-40 lysis buffer from UM-PDX-HACC-5 tumor tissue or UM-HACC cells plated at 2×10^5 cells per 60 mm^3 dishes and grown to 90% confluence in SGM. Lysates were analyzed by PAGE and membranes were blocked for 60 minutes in 5% milk in TBST. Membranes were probed with antibodies to MDM2, p53, EGFR, E-Cadherin, B-actin (Santa Cruz Biotechnology), phospho-p53 (S392), or p21 (Cell Signaling) in TBST, overnight at 4°C. For dose response studies, 2×10^5 cells were plated, attached overnight, treated in fresh medium with 0 to 10 μmol/L MI-773 for 24 hours. Immunohistochemistry was performed on vehicle and MI-773–treated tumors to detect p53, and cytokeratin-7 (Cell Signaling) using standard methods. TUNEL analysis was performed according to manufacturer's instruction using an *in situ* Cell Death Detection Kit (Roche). Morphometric image analysis was performed for cells undergoing apoptosis or expressing p53 using the software Image-J (NIH, Bethesda, MD). Images of 10 fields of each slide (three slides per group) were captured at 400× magnification using a QImaging-ExiAqua monochrome digital camera attached to a Nikon Microscope (Nikon) and visualized with QCapturePro software. All positive and negative cells were counted in each field and the percentage of total number of positive cells was calculated. Fluorescence *in situ* hybridization (FISH) analysis was performed using a centromeric BAC probe labeled in fluorescein and a telomeric BAC probe labeled with 5-Rox (red), as described (19).

Cytotoxicity, flow cytometry, and p53 gene silencing

Sulforhodamine B (SRB) or the WST-1 (Roche) cytotoxicity assay were performed to determine the effect of MI-773 on ACC cell viability, as we described (24). Briefly, 1 to 3×10^3 UM-HACC cells were plated per well, and treated with 0 to 40 μmol/L MI-773 for 24 to 96 hours. To assess apoptosis, 2×10^5 cells were plated in 60 mm^3 dishes, attached overnight, and treated with 0 to 20 μmol/L MI-773 for 72 hours. Cells were lysed with a hypotonic buffer and stained with propidium iodide, as described (24). Primary low passage ACC cells (UM-HACC-5) were stably transduced with lentiviral vectors expressing shRNA-p53 or scrambled sequence control shRNA-C (University of Michigan Vector Core) and selected with 1.0 μg/mL puromycin (Sigma).

Statistical analyses

Censored survival estimates were determined using Kaplan–Meier curves and statistical significance was determined using log rank (Mantel–Cox) test. Tumor growth inhibition (TGI) was calculated using the formula: 1 − [(Treated final − Treated initial)/(Control final − Control initial)]. Percent shrinkage was determined by 1 − (Treated final – Treated initial) × 100. One-way ANOVA, followed by *post hoc* tests (Tukey test), Mann–Whitney *U*-test, or Student *t*-test were used to determine significant differences in tumor growth, weight, volume, apoptosis levels, cell viability, TUNEL, and p53 expression in control and treated tumors. Significance was determined at $P < 0.05$.

Results

Establishment and characterization of a PDX model of ACC

To establish the UM-PDX-HACC-5 model, we transplanted human tumor fragments into SCID mice (Supplementary Fig. S1). Two oral pathologists (FN, MDM) evaluated the histopathology of these tumors and observed a tubular-cribriform pattern with areas of perineural invasion (Supplementary Fig. S1A), which is representative of the typical pathobiology of ACC. The first passage xenograft tumors showed similar histopathologic patterns to the human tumor. With increasing *in vivo* passages, the PDX tumors acquired a more solid subtype with frequent mitotic figures and cellular pleomorphism, which correlated with a sharp increase in tumor growth rates and tumor take (Supplementary Fig. S1A and S1B). Although first passage tumors reached 600 to 900 mm^3 within 70 to 84 days, higher passage tumors reached similar size in approximately 35 to 40 days (Supplementary Fig. S1B). Notably, tumor take was consistently high (93/113, 82.3%) for this model (Supplementary Fig. S1C).

To determine if UM-PDX-HACC-5 tumors had the MYB–NFIB translocation, fluorescent *in situ* hybridization (FISH) analysis was performed on passage 3 tumors. The break-apart photo shows at least two cells with two fused red/green signals indicating intact MYB loci. The fusion FISH photo shows a representative cell with distinct green and red signals indicating the 2 genes remain separate (Supplementary Fig. S1D). These results indicate that the UM-PDX-HACC-5 model is representative of the 30% to 40% of ACC that do not have the MYB–NFIB translocation. Notably, we observed that the expression of key targets of MI-773 (i.e., MDM2, p53, p63) is relatively stable over *in vivo* passaging (Supplementary Fig. S1E).

Figure 1.

MI-773 induces tumor regression in UM-PDX-HACC-5, a PDX model of ACC. A, graph depicting average tumor volume in mice that received 10, 100 mg/kg MI-773 or vehicle via daily oral gavage for 20 days. Treatment started when tumors were approximately 200 mm^3. *, $P < 0.05$. B, Kaplan–Meier analysis of time to failure, as defined by doubling tumor volume as compared to pretreatment volume ($n = 6$–8/group). C, photographs of the mice and tumors immediately after euthanasia. D, graphs depicting actual weight and volume of tumors retrieved from the mice at the termination of the experiment. E, graph depicting mouse weight for the duration of the experiment.

Published OnlineFirst March 2, 2016; DOI: 10.1158/1078-0432.CCR-15-1698

Table 1. Table showing tumor growth inhibition (TGI) index and percent tumor shrinkage in mice treated with vehicle, 10, 100 mg/kg MI-773, as compared to pretreatment volumes

Treatment	Dose (mg/kg)	Route/schedule	Pretreatment (mean ± SD)	Final (mean ± SD)	Mean difference	TGI	Shrinkage (%)
Vehicle	0	P.O.; daily	167.2 ± 90.1	934.9 ± 936.0	+767.7	–	NA
MI-773	10	P.O.; daily	239.2 ± 51.4	740.3 ± 350.2	+501.1	34	NA
MI-773	100	P.O.; daily	242.3 ± 80.9	33.0 ± 4.9	−209.2	127	86

NOTE: TGI greater than 50 is typically considered significant.

MI-773 promotes ACC tumor regression

To evaluate the antitumor effect of MI-773, PDX tumors were transplanted into SCID mice, allowed to grow to an average of 250 mm^3, and then mice were treated with 0 to 100 mg/kg MI-773. MI-773 at 10 mg/kg modestly reduced the rate of tumor growth, whereas 100 mg/kg caused significant tumor regression (Fig. 1A). Control tumors reached an average of 1,000 mm^3 at 20 days of treatment, compared to an average volume of 600 mm^3 for the 10 mg/kg group and 30 mm^3 for the 100 mg/kg group. Kaplan–Meier analysis showed an increase in tumor failure, defined as two times increase in tumor volume as compared to pretreatment volume ($P = 0.044$), for vehicle-treated mice when compared to mice treated with 100 mg/kg MI-773 (Fig. 1B and C). These data were confirmed by the evaluation of tumor weight and volume at the end of the experiment (Fig. 1D). MI-773 was well tolerated by the mice, as shown by the lack of observable weight loss during the experimental period (Fig. 1E). To better understand the antitumor effect of MI-773 in preclinical models of ACC, the tumor growth inhibition (TGI) index was calculated for each treatment condition. Although 10 mg/kg MI-773 mediated a TGI of 34%, 100 mg/kg MI-773 had a TGI of 127%, with robust tumor shrinkage of 86% (Table 1). Two additional PDX models of ACC (ACCx6 and ACCx9; ref.19) were used to verify the scope of the antitumor effect of MI-773. We observed that MI-773 mediated tumor regression in the ACCx6 model ($P = 0.044$) and in the ACCx9 model ($P = 0.012$), as compared to vehicle-treated controls (Fig. 2A and B). As expected, MI-773 was well tolerated in these mice, as demonstrated by maintenance of body weight in the treatment group (Fig. 2C and D).

To further verify the antitumor effect of MI-773, two independent experiments were performed using the UM-PDX-HACC-5 model. Again, 100 mg/kg MI-773 mediated potent tumor regression (Supplementary Figs. S2A, S2D, S2F and S3A, S3D, S3F). Treated tumors were visibly smaller, and mice did not lose weight upon treatment (Supplementary Figs. S2C, S2E and S3C, S3E). We noted that 10 or 50 mg/kg MI-773 were not sufficient to cause significant tumor regression, suggesting that a higher dose (e.g., 100 mg/kg) is necessary for measurable antitumor effect in mice (Fig. 1A and Supplementary Fig. S3A). Kaplan–Meier analyses confirmed that 100 mg/kg MI-773 prevents tumor failure, when compared to vehicle or lower dose MI-773 (Supplementary Figs. 2SB and 3SB). Taken together, these data demonstrate that single-agent MI-773 mediates ACC tumor regression without observable systemic cytotoxicity in mice.

MI-773 induces ACC apoptosis

To begin to evaluate possible mechanisms of MI-773–induced ACC tumor regression, we performed *in situ* TUNEL analysis (Fig. 3A) in tissues collected from mice treated in the experiment showed in Figure 1. The percentage of apoptotic cells in the MI-773–treated tumors was higher ($P = 0.015$) than in tumors from vehicle-treated mice (Fig. 3B). To further understand mechanisms of MI-773–induced ACC cell death, we performed viability assays on low passage UM-HACC-5 cells that showed low micromolar IC_{50} for MI-773 upon 48 or 96 hours of treatment (Fig. 3C). We also observed a dose-dependent induction of UM-HACC-5 apoptosis after 72 hours (Fig. 3D) that was accompanied by a gradual decrease in the fraction of cells in G_2–M phase of cell cycle (Fig. 3E). Additional cell viability assays performed in UM-HACC-5 and UM-HACC-6 cells *in vitro* showed similar trends of response to MI-773 treatment (Supplementary Fig. S4A and S4B). To verify the dependency of MI-773's effect on the function of p53, we partially silenced p53 expression in UM-HACC-5 cells with an shRNA-p53 construct. We observed that p53-silenced cells exhibit a higher IC_{50} than shRNA-C control cells (Supplementary Fig. S4C–S4E).

Histopathologic characteristics associated with MI-773–induced tumor regression

To improve the characterization of the tumors treated with MI-773, two oral pathologists (FN, MDM) performed histopathologic analysis of tissue specimens upon termination of treatment. In vehicle control tumors, intense cellular pleomorphism, cells with large and/or hyperchromatic nucleus, prominent nucleoli, and loosely packed chromatin, altered nuclear–cytoplasmic ratio, and frequent infiltration in muscle, nerve, and adipose tissue were observed (Supplementary Fig. S5A). The morphology of tumors treated with MI-773 was very different: round cells exhibited a vacuolated cytoplasm and many granules were surrounded by a hyaline connective tissue (Supplementary Fig. S5B). Treated tumors did not invade into adjacent muscle tissue, but infiltration of tumor cells into nerve and adipose tissues were present in some areas. To confirm that the unusual-shaped cells were indeed epithelial, immunohistochemical staining was performed and showed high cytokeratin-7 positivity in both vehicle and MI-773–treated tumors (Fig. 4A). Immunohistochemical staining also showed more p53-positive cells in MI-773–treated tumors than in vehicle control tumors ($P < 0.001$; Fig. 4A and B). Notably, although most of the vehicle-treated tumors exhibited p53 primarily localized in the nucleus, tumors treated with MI-773 showed primarily cytoplasmic localization of p53 (Fig. 4A and C). In addition, increased levels of p53 and phospho-p53 (S392) proteins were detected in tumors treated with MI-773, when compared to vehicle tumors (Fig. 4D).

MI-773 potently activates MDM2, p53, and p21 in low passage ACC cells

Low passage ACC cells were screened by Western blot for basal levels of p53, EGFR, and ECAD, using as controls two mucoepidermoid carcinoma cell lines (UM-HMC-3A, UM-HMC-3B) previously characterized in our laboratory

Published OnlineFirst March 2, 2016; DOI: 10.1158/1078-0432.CCR-15-1698

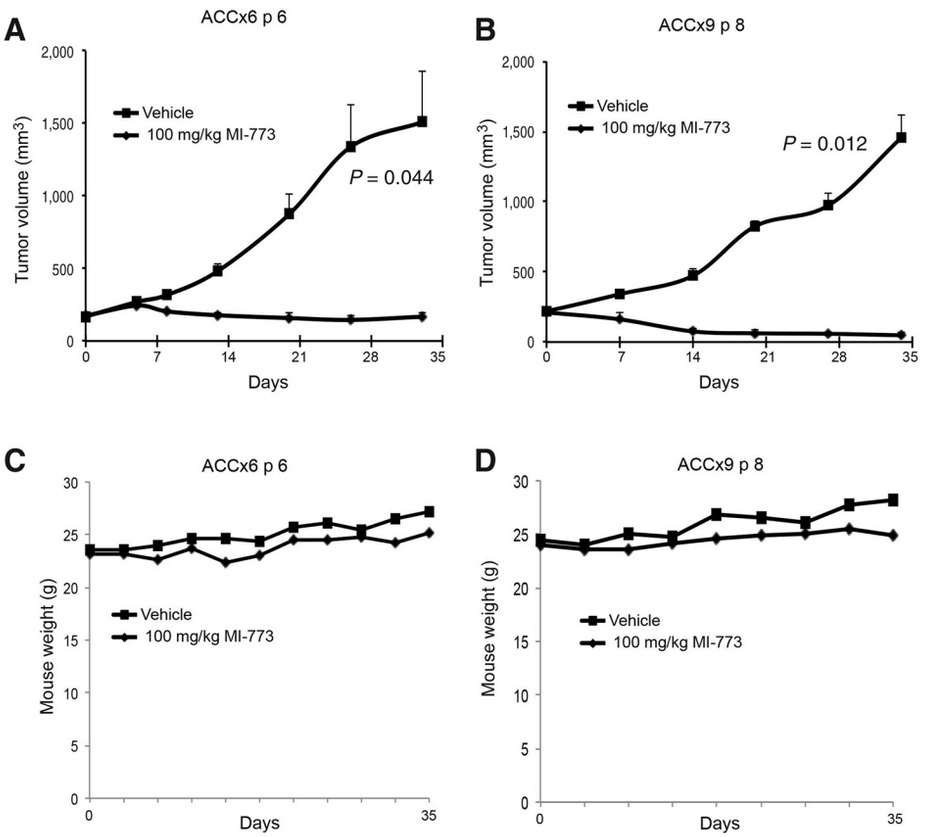

Figure 2.
MI-773 induces tumor regression in two additional PDX models of ACC. A, B, graphs depicting average tumor volume in mice harboring ACCx6 (A) or ACCx9 (B) that received 100 mg/kg MI-773 or vehicle via daily oral gavage. Treatment started when tumors were approximately 200 mm^3. C, D, graphs depicting mouse weight for the duration of the experiment.

(15). We observed that baseline p53 levels varied according to cell line, but they were relatively stable over different passages in most cell lines (Fig. 5A and B). EGFR and ECAD expression levels were lower in UM-HACC-2B cells than in the other UM-HACC cells (Fig. 5A), and highly expressed in UM-HMC-3A and UM-HMC-3B, as previously reported (15). We then evaluated the effect of MI-773 on the activation of key downstream effectors and observed a potent and dose-dependent activation of MDM2, p53, and p21 in all five low passage primary human ACC cell lines evaluated here (Fig. 5C). We also observed an overall pattern of induction of p53 phosphorylation at serine 392 promoted by increasing concentrations of MI-773 (Fig. 5D). These results suggested that the p53 axis is functional in the ACC models studied here. Nevertheless, we performed DNA sequencing that showed wild-type TP53 gene in all ACC models used here, except for a possible polymorphism at position 72 in the UM-HACC-5 cells that was not observed in the correspondent UM-PDX-HACC-5 model (Supplementary Fig. S6). Taken together, these data support a potent and specific pro-apoptotic effect of MI-773 mediated by the activation of the p53 signaling axis in several preclinical models of human ACC.

Discussion

A cure is typically not achievable for many patients with ACC due to the lack of effective and safe systemic antitumor agents for this malignancy. The lack of experimental models has hindered progress in the discovery of therapies for this cancer. Patients are left without alternatives beyond surgery (when possible) and radiation. Here we characterize a new PDX model of ACC, and used two previously established models of ACC (19), to test a novel potent and specific small molecule inhibitor of the MDM2–p53 interaction.

The UM-PDX-HACC-5 model was generated from an ACC located in a minor salivary gland from the hard palate that exhibited a primarily solid histopathologic subtype, which correlates with more aggressive disease in humans (1). PDX tumors at *in vivo* passages 2 and higher grew to 2,000 mm^3 within 30 days, exhibiting a vigorous growth pattern characteristic of highly aggressive tumors. We consider this model uniquely suited for developmental therapeutic studies because it is very aggressive, and therefore it provides a rigorous platform for the testing of new anticancer drugs. To better mimic epidemiological realities and clinical scenarios, we chose to perform our experiments in female mice reflecting the fact that ACC is more common in women (25). In addition, the work with the UM-PDX-HACC-5 model, we also tested MI-773 in ACCx6 PDX tumors derived from a lung metastasis (grade 2) and in the ACCx9 PDX model developed from a primary parotid tumor (grade 3). It is well-known that a specific gene translocation identified as t(6:9) results in the fusion of MYB proto-oncogene with the transcription factor NFIB and is rather frequent in ACCs (26–28). This translocation is detected in ACCx9 tumors, but was not present in ACCx6 (19) or UM-PDX-HACC-5 tumors. Therefore, the preclinical models used here represent a diverse panel of ACC tumors that is perhaps representative of the typical diversity of presentation of this disease.

Published OnlineFirst March 2, 2016; DOI: 10.1158/1078-0432.CCR-15-1698

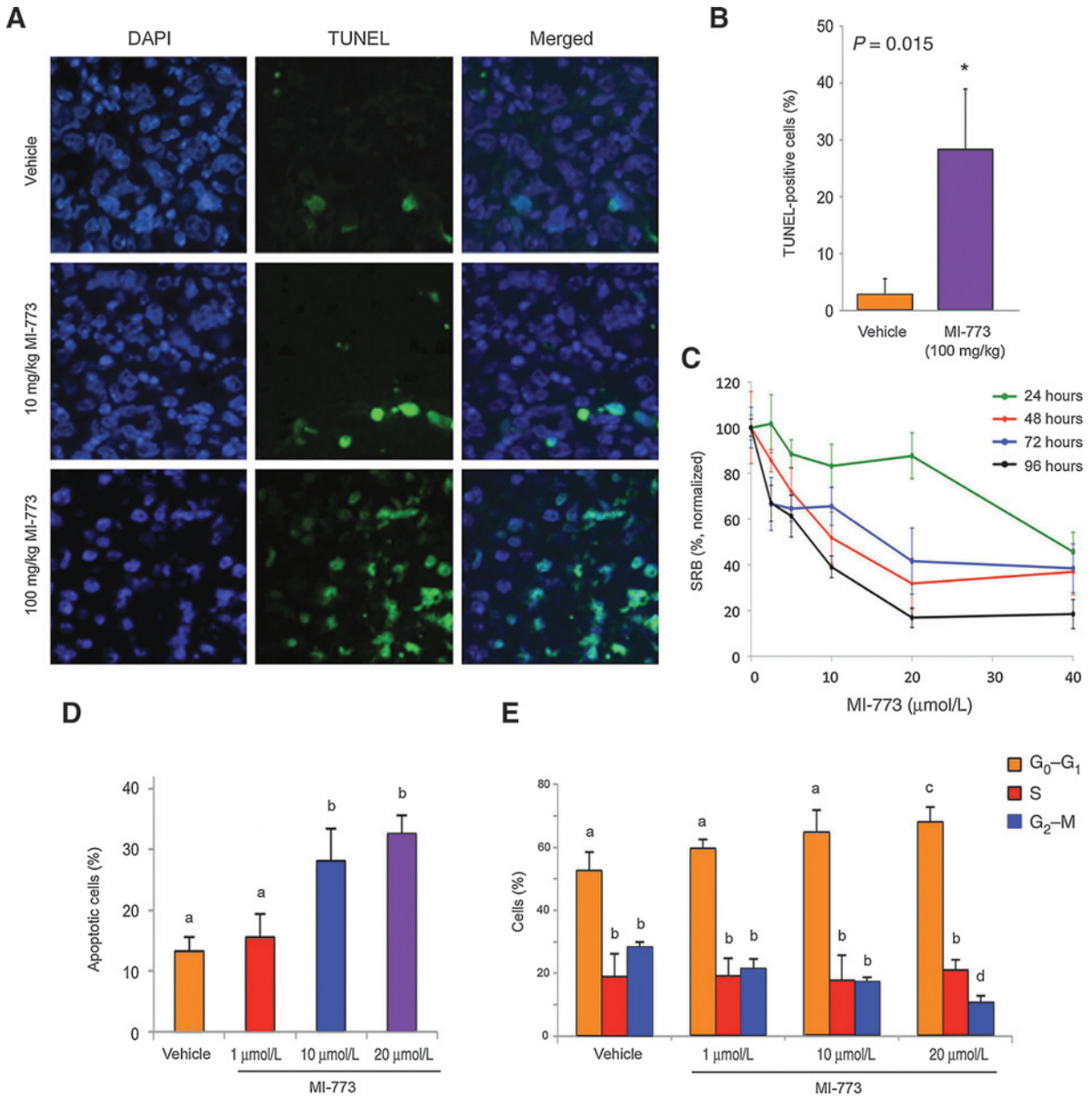

Figure 3.
MI-773 induces tumor cell apoptosis. A, photomicrographs of TUNEL-positive cells (green) and DAPI (blue) in tumors from mice that received vehicle, 10 or 100 mg/kg MI-773. B, graph depicting the percentage of TUNEL-positive cells from tumors represented in A. C, graph depicting toxicity of MI-773 in UM-HACC-5 cells *in vitro*, as determined by SRB assay. D, graph depicting the fraction of apoptotic cells after 72 hours of treatment with MI-773, as determined by the fraction of cells in sub-G_0–G_1 after propidium iodide staining. E, graph depicting the fraction of cells/cell cycle phase after 72 hours of treatment with MI-773, as determined by propidium iodide staining. Different lower case letters represent $P < 0.05$.

MI-773–mediated potent tumor regression in the three PDX models evaluated here, despite differences in tumor site, grade, or MYB-NFIB status. Indeed, we observed robust and unequivocal tumor regression caused by single-agent MI-773 in several independent experiments. Notably, the tumor regression observed here was not accompanied by objective signs of systemic toxicities, as shown by the maintenance of mouse weight throughout the experimental period.

The histopathologic changes reported here correlated with a significant increase in p53 expression and a shift in the localization of p53 from the nucleus to the cytoplasm in tumors treated with MI-773. It is well known that p53 has multiple roles depending on its cellular location and level of activation (29–31). When located in the nucleus, p53 functions primarily as a transcription factor to induce expression of several proteins related to cell signaling, angiogenesis, autophagy, and apoptosis. Cytoplasmic functions of p53 include transcription-independent mechanisms to induce apoptosis by interacting directly with pro-apoptotic proteins (29–31). The correlation of significant induction of apoptosis with the

Published OnlineFirst March 2, 2016; DOI: 10.1158/1078-0432.CCR-15-1698

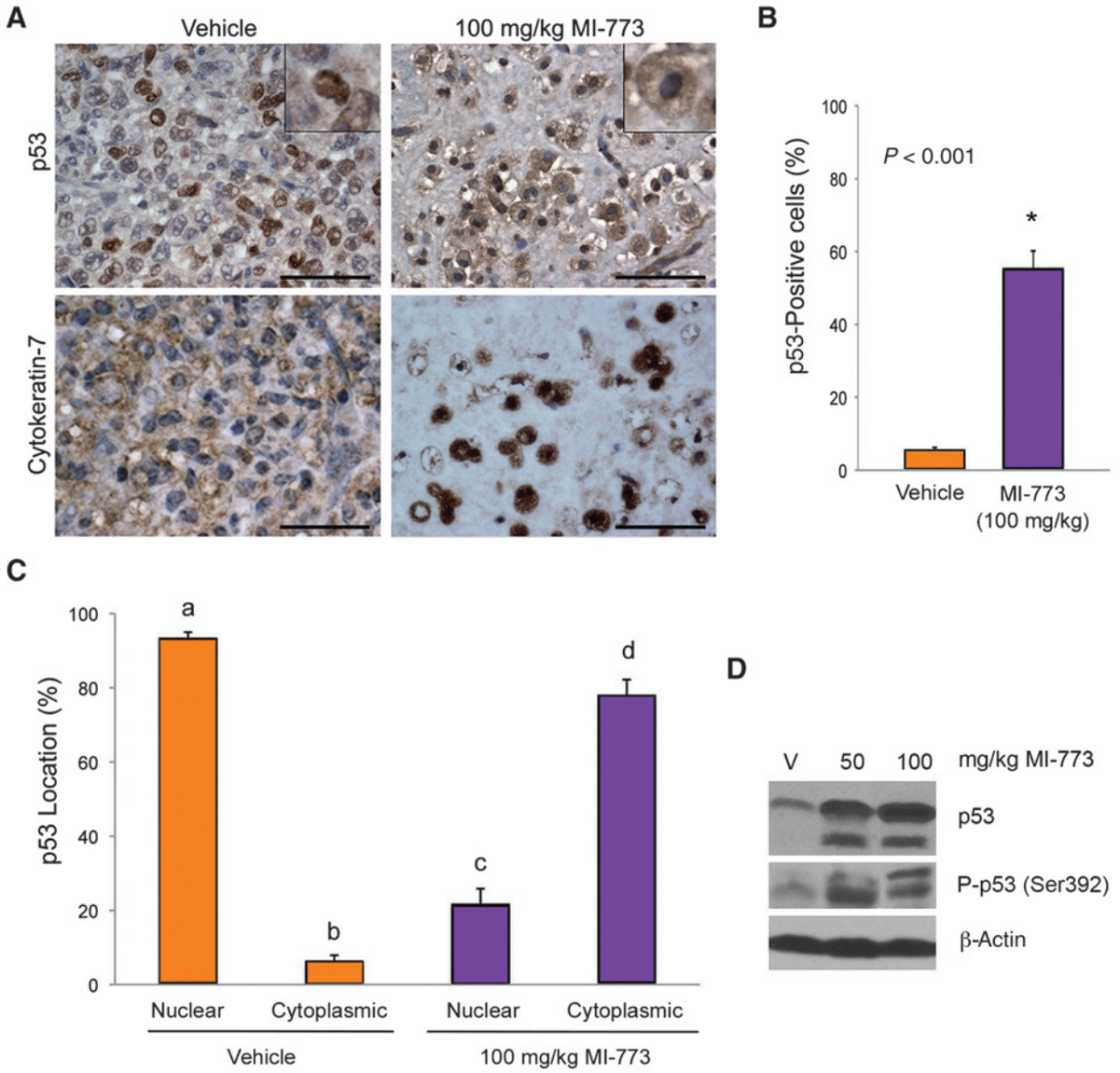

Figure 4.
MI-773 induces p53 expression in ACC tumors *in vivo*. A, photomicrographs of immunohistochemistry for p53 and cytokeratin 7 in vehicle or 100 mg/kg MI-773–treated tumors. Inserts depict representative cells at high magnification. Note the shift of p53 from the nucleus (vehicle group) to the cytoplasm (MI-773-treated group). B, graph depicting the percentage of p53-positive cells in ACC tumors represented in A. $P < 0.05$. C, graph depicting the localization of p53 (nucleus or cytoplasm) in tumors retrieved from mice that received vehicle or 100 mg/kg MI-773. Different lower case letters represent $P < 0.05$. Scale bars = 50 μm. D, Western blot showing p53 and phospho-p53 (Ser392) in whole tumor lysates prepared from mice that received vehicle, 50, or 100 mg/kg MI-773.

shuttling of p53 from the nucleus to the cytoplasm upon treatment with MI-773 suggests that this small molecule inhibitor is working through transcription-independent mechanisms to induce tumor cell death *in vivo*.

Results from our *in vivo* experiments, and particularly the Western blots performed with a panel of primary human low passage ACC cells demonstrated a potent, dose-dependent activation of p53 and its downstream transcriptional targets p21 and MDM2. We also observed potent induction of phosphorylation of p53 at the Serine 392 position by MI-773. This is considered a common site for p53 phosphorylation by various therapeutic agents, such as etoposide, UV, ionizing radiation, and Nutlin3, another inhibitor of the MDM2–p53 interaction (32, 33). Collectively, these data provide support to the specific effect of MI-773 on its expected targets, and suggest the function of wild-type p53 in these cells (20). Indeed, gene sequencing revealed that the TP53 gene was not mutated in any of the ACC models evaluated here. The only change that we observed was a polymorphism at amino acid 72 that was detected in our UM-HACC-5 low passage cells. This polymorphism (arginine

Published OnlineFirst March 2, 2016; DOI: 10.1158/1078-0432.CCR-15-1698

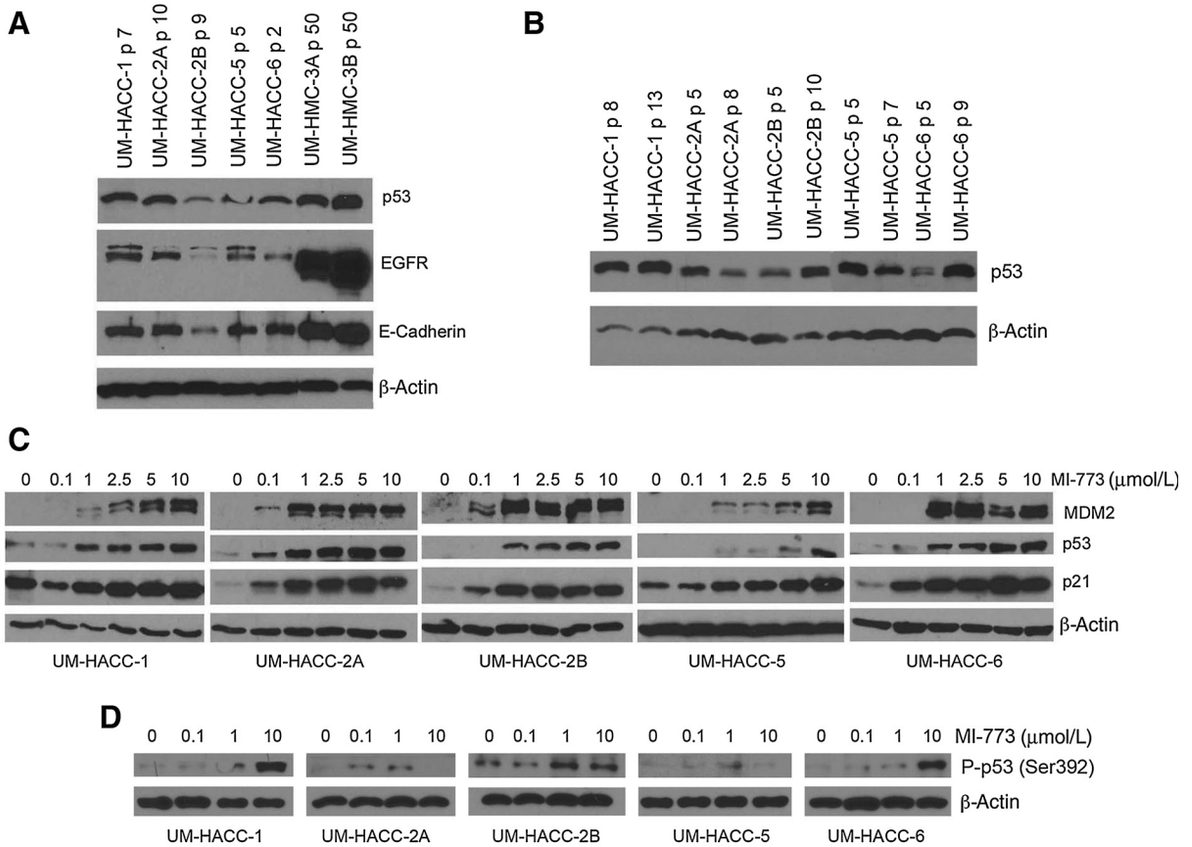

Figure 5.
Effect of MI-773 on its targets and downstream effectors in ACC tumor cells *in vitro*. A, Western blot for p53, EGFR, and E-Cadherin in a panel of low passage primary human cells (UM-HACC series). Mucoepidermoid carcinoma cells (UM-HMC-3A,-3B) served as controls for p53, EGFR, and E-Cadherin. B, Western blots showing levels of p53 over different passages in a panel of primary human ACC cells. C, D, Western blots for MDM2, p53, p21, and phospho-p53 (Ser392) expression upon treatment with increasing concentrations of MI-773 (24 hours) in a panel of low passage UM-HACC cells.

or proline) has been well documented as having no impact on p53 function (34, 35).

In summary, we present here strong preclinical evidence for the therapeutic potential of the new small molecule inhibitor of the MDM2–p53 interaction (MI-773) in ACC. The development of potent inhibitors of MDM2 is an area of intense research today, as demonstrated by the fact that seven small molecule inhibitors of MDM2 (including MI-773) are currently in clinical trials (33). Considering the potent tumor regression observed with single-agent MI-773 in models of aggressive ACC, it is tempting to say that MDM2 inhibition may offer the first effective therapy for these patients. This hypothesis, however, will have to be challenged in well-conducted randomized clinical trials.

Disclosure of Potential Conflicts of Interest

C.A. Moskaluk is a consultant/advisory board member for Novartis. S. Wang has ownership interest (including patents) in Ascenta Therapeutics, and reports receiving commercial research grants from Ascenta Therapeutics/Sanofi. No potential conflicts of interest were disclosed by the other authors.

Authors' Contributions

Conception and design: G.A. Acasigua, J.E. Nör

Development of methodology: K.A. Warner, G.A. Acasigua, Z. Zhang, M.J. Wick, J.E. Nör

Acquisition of data (provided animals, acquired and managed patients, provided facilities, etc.): K.A. Warner, F. Nör, G.A. Acasigua, M.D. Martins, M.E. Spector, J. Helman, M.J. Wick, C.A. Moskaluk, R.M. Castilho, A.T. Pearson, J.E. Nör

Analysis and interpretation of data (e.g., statistical analysis, biostatistics, computational analysis): K.A. Warner, F. Nör, G.A. Acasigua, M.D. Martins, C.A. Moskaluk, R.M. Castilho, A.T. Pearson, J.E. Nör

Writing, review, and/or revision of the manuscript: K.A. Warner, F. Nör, G.A. Acasigua, S.A. McLean, M.E. Spector, D.B. Chepeha, A.T. Pearson, J.E. Nör

Administrative, technical, or material support (i.e., reporting or organizing data, constructing databases): K.A. Warner, M.E. Spector, D.B. Chepeha, J.E. Nör

Study supervision: J.E. Nör

Other (technical assistance and data analysis): Z. Zhang

Other (specimen collection): D.B. Chepeha

Other (providing the drug): S. Wang

Acknowledgments

The authors thank the patients who kindly provided the tumor specimens used to generate the ACC cells and PDX models that enabled this research project. The authors also thank the surgeons, nurses, and support staff that enabled the process of tumor specimen collection and processing for use in research. The authors also thank Jeffrey Kaufman and the Adenoid Cystic Carcinoma Research Foundation (AACRF)

for the strong support and encouragement received throughout this project.

Grant Support

This work was funded by a grant from the Adenoid Cystic Carcinoma Research Foundation (AACRF); University of Michigan Head Neck SPORE P50-CA-97248 from the NIH/NCI; and grants R01-DE23220, R01-DE21139 from the NIH/NIDCR (JEN).

The costs of publication of this article were defrayed in part by the payment of page charges. This article must therefore be hereby marked *advertisement* in accordance with 18 U.S.C. Section 1734 solely to indicate this fact.

Received July 16, 2015; revised January 14, 2016; accepted February 8, 2016; published OnlineFirst March 2, 2016.

References

1. Seethala RR. An update on grading of salivary gland carcinomas. Head Neck Pathol 2009;3:69–77.
2. Simpson RH, Skálová A, Di Palma S, Leivo I. Recent advances in the diagnostic pathology of salivary carcinomas. Virchows Arch 2014;465: 371–84.
3. Kowalski PJ, Paulino AF. Perineural invasion in adenoid cystic carcinoma: its causation/promotion by brain-derived neurotrophic factor. Hum Pathol 2002;33:933–6.
4. Marchiò C, Weigelt B, Reis-Filho JS. Adenoid cystic carcinomas of the breast and salivary glands (or `The strange case of Dr. Jekyll and Mr. Hyde' of exocrine gland carcinomas). J Clin Pathol 2010;63:220–8.
5. Dodd RL, Slevin NJ. Salivary gland adenoid cystic carcinoma: a review of chemotherapy and molecular therapies. Oral Oncol 2006;42:759–69.
6. Milano A, Longo F, Basile M, Iaffaioli RV, Caponigro F. Recent advances in the treatment of salivary gland cancers: emphasis on molecular targeted therapy. Oral Oncol 2007;43:729–34.
7. Hainaut P, Hollstein M. p53 and human cancer: the first ten thousand mutations. Adv Cancer Res 2000;77:81–137.
8. Daujat S, Neel H, Piette J. MDM2: life without p53. Trends Genet 2001; 17:459–64.
9. Cahilly-Snyder L, Yang-Feng T, Francke U, George DL. Molecular analysis and chromosomal mapping of amplified genes isolated from a transformed mouse 3T3 cell line. Somat Cell Mol Genet 1987;13:235–44.
10. Jin L, Xu L, Song X, Wei Q, Sturgis EM, Li G. Genetic variation in MDM2 and p14ARF and susceptibility to salivary gland carcinoma. PLoS One 2012;7:e49361.
11. Abd-Elhamid ES, Elmalahy MH. Image cytometric analysis of p53 and mdm-2 expression in primary and recurrent mucoepidermoid carcinoma of parotid gland: immunohistochemical study. Diagn Pathol 2010;5:1–13.
12. Matizonkas-Antonio LF, de Mesquita RA, de Souza SC, Nunes FD. TP53 mutations in salivary gland neoplasms. Braz Dent J 2005;16:162–6.
13. de Araújo VC, Martins MT, Leite KR, Gomez RS, de Araújo NS. Immunohistochemical Mdm2 expression in minor salivary gland tumours and its relationship to p53 gene status. Oral Oncol 2000;36:67–9.
14. de Lima Mde D, Marques YM, Alves Sde M Jr, Freitas VM, Soares FA, de Araújo VC, et al. MDM2, P53, P21WAF1 and pAKT protein levels in genesis and behaviour of adenoid cystic carcinoma. Cancer Epidemiol 2009; 33:142–6.
15. Warner KA, Adams A, Bernardi L, Nor C, Finkel KA, Zhang Z, et al. Characterization of tumorigenic cell lines from the recurrence and lymph node metastasis of a human salivary mucoepidermoid carcinoma. Oral Oncol 2013;49:1059–66.
16. Phuchareon J, Ohta Y, Woo JM, Eisele DW, Tetsu O. Genetic profiling reveals cross-contamination and misidentification of 6 adenoid cystic carcinoma cell lines: ACC2, ACC3, ACCM, ACCNS, ACCS, and CAC2. PLoS One 2009;4:e6040.
17. Queimado L, Lopes C, Du F, Martins C, Fonseca I, Bowcock AM, et al. *In vitro* transformation of cell lines from human salivary gland tumors. Int J Cancer 1999;81:793–8.
18. Li J, Perlaky L, Rao P, Weber RS, El-Naggar AK. Development and characterization of salivary adenoid cystic carcinoma cell line. Oral Oncol 2014;50:991–9.
19. Moskaluk CA, Baras AS, Mancuso SA, Fan H, Davidson RJ, Dirks DC, et al. Development and characterization of xenograft model systems for adenoid cystic carcinoma. Lab Invest 2011;91:1480–90.
20. Wang S, Sun W, Zhao Y, McEachern D, Meaux I, Barrière C, et al. SAR405838: an optimized inhibitor of MDM2-p53 interaction that induces complete and durable tumor regression. Cancer Res 2014;74: 5855–65.
21. Yu S, Qin D, Shangary S, Chen J, Wang G, Ding K, et al. Potent and orally active small-molecule inhibitors of the MDM2-p53 interaction. J Med Chem 2009;52:7970–3.
22. Azmi AS, Aboukameel A, Banerjee S, Wang Z, Mohammad M, Wu J, et al. MDM2 inhibitor MI-319 in combination with cisplatin is an effective treatment for pancreatic cancer independent of p53 function. Eur J Cancer 2010;46:1122–31.
23. Zhao Y, Yu S, Sun W, Liu L, Lu J, McEachern D, et al. A potent small-molecule inhibitor of the MDM2-p53 interaction (MI-888) achieved complete and durable tumor regression in mice. J Med Chem 2013;56: 5553–61.
24. Zeitlin BD, Joo E, Dong Z, Warner K, Wang G, Nikolovska-Coleska Z, et al. Antiangiogenic effect of TW37, a small-molecule inhibitor of Bcl-2. Cancer Res 2006;66:8698–706.
25. Boukheris H, Curtis RE, Land CE, Dores GM. Incidence of carcinoma of the major salivary glands according to the WHO classification, 1992 to 2006: a population-based study in the United States. Cancer Epidemiol Biomarkers Prev 2009;18:2899–906.
26. Brill LB 2nd, Kanner WA, Fehr A, Andrén Y, Moskaluk CA, Löning T, et al. Analysis of MYB expression and MYB-NFIB gene fusions in adenoid cystic carcinoma and other salivary neoplasms.Mod Pathol 2011;24:1169–76.
27. West RB, Kong C, Clarke N, Gilks T, Lipsick JS, Cao H, et al. MYB expression and translocation in adenoid cystic carcinomas and other salivary gland tumors with clinicopathologic correlation.Am J Surg Pathol 2011;35:92–9.
28. Persson M, Andrén Y, Mark J, Horlings HM, Persson F, Stenman G. Recurrent fusion of MYB and NFIB transcription factor genes in carcinomas of the breast and head and neck. Proc Natl Acad Sci U.S.A. 2009;106: 18740–4.
29. Green DR, Kroemer G. Cytoplasmic functions of the tumour suppressor p53. Nature 2009;458:1127–30.
30. Vaseva AV, Moll UM. The mitochondrial p53 pathway. Biochim Biophys Acta 2009;1787:414–20.
31. Speidel D. Transcription-independent p53 apoptosis: an alternative route to death. Trends Cell Biol 2010;20:14–24.
32. Cox ML, Meek DW. Phosphorylation of serine 392 in p53 is a common and integral event during p53 induction by diverse stimuli. Cell Signal 2010; 22:564–71.
33. Zhao Y, Aguilar A, Bernard D, Wang S. Small-molecule inhibitors of the MDM2-p53 protein-protein interaction (MDM2 Inhibitors) in clinical trials for cancer treatment. J Med Chem 2015;58:1038–52.
34. Whibley C, Pharoah PD, Hollstein M. p53 polymorphisms: cancer implications. Nat Rev Cancer 2009;9:95–107.
35. Thomas M, Kalita A, Labrecque S, Pim D, Banks L, Matlashewski G. Two polymorphic variants of wild-type p53 differ biochemically and biologically. Mol Cell Biol 1999;19:1092–100.

Published OnlineFirst March 2, 2016; DOI: 10.1158/1078-0432.CCR-15-1698

Clinical Cancer Research

Targeting MDM2 for Treatment of Adenoid Cystic Carcinoma

Kristy A. Warner, Felipe Nör, Gerson A. Acasigua, et al.

Clin Cancer Res 2016;22:3550-3559. Published OnlineFirst March 2, 2016.